Available online at www.sciencedirect.com

SciVerse ScienceDirect

Physics Procedia 20 (2011) 6–23

Physics Procedia

Space, Propulsion & Energy Sciences International Forum - 2011

Vortex Formation in the Wake of Dark Matter Propulsion

G. A. Robertson[a]*, M. J. Pinheiro[b]

[a]*Institute for Advanced Studies in the Space, Propulsion & Energy Sciences, 265 Ita Ann, Madison, AL 35757, USA*
[b]*Department of Physics & Institute of Plasma and Nuclear Fusion, Instituto Superior Tecnico, Av. Rovisco Pais, 1049-001 Lisboa, Portugal*

Abstract

Future spaceflight will require a new theory of propulsion; specifically one that does not require mass ejection. A new theory is proposed that uses the general view that closed currents pervade the entire universe and, in particular, there is a cosmic mechanism to expel matter to large astronomical distances involving vortex currents as seen with blazars and blackholes. At the terrestrial level, force producing vortices have been related to the motion of wings (e.g., birds, duck paddles, fish's tail). In this paper, vortex structures are shown to exist in the streamlines aft of a spaceship moving at high velocity in the vacuum. This is accomplished using the density excitation method per a modified Chameleon Cosmology model. This vortex structure is then shown to have similarities to spacetime models as Warp-Drive and wormholes, giving rise to the natural extension of Hawking and Unruh radiation, which provides the propulsive method for space travel where virtual electron-positron pairs, absorbed by the gravitational expansion forward of the spaceship emerge from an annular vortex field aft of the spaceship as real particles, in-like to propellant mass ejection in conventional rocket theory.

© 2011 Published by Elsevier B.V. Open access under CC BY-NC-ND license.
Selection and/or peer-review under responsibility of the Organising Committee of the ICOPEN 2011 conference

PACS: 40., 11.90.+t, 13.40.-f, 47.57.jd, 47.65.-d
Keywords: Electromagnetism; Classical Mechanics; Fluid Dynamics; Other Topics in General Theory of Fields and Particles; Electromagnetic Processes and Properties; Electrokinetic Effects; Magnetohydrodynamics and Electrohydrodynamics

1. Introduction

Future spaceflight will require a new theory of propulsion; specifically, one that does not require mass ejection. In a recent paper [1], the second author introduce the concept of electromagnetotoroid in astrophysics and its role in polar jets, showing that it represents the onset of Abraham's force driven by

* Corresponding author. Tel.: +1-256-694-7941; fax: +0-000-000-0000 .
E-mail address: gar@ias-spes.org .

1875-3892 © 2011 Published by Elsevier B.V. Selection and/or peer-review under responsibility of Institute for Advanced studies in Space, Propulsion and Energy Sciences Open access under CC BY-NC-ND license.
doi:10.1016/j.phpro.2011.08.002

some external source. He further showed that the Abraham's force term is the analogue of the Magnus force, and thus represents the formation of vortex structures, of electromagnetic nature, in the fabric of space-time. This was shown to prove that major natural propulsion processes on Earth (*e.g*., birds, fishes) and in the Universe (*e.g*., Herbig-Haro objects as seen with blazars and blackholes) all have the same underlying vortex nature at their base.

Over the last few years, the first author [2-4] introduced a modified Chameleon (Cosmology) model for use in propulsion derived from the Khoury and Weltman Chameleon (Cosmology) Theory [5, 6]. The Chameleon theory is a dark matter/energy theory that assumes forces from the change in densities in or about an object. In this paper, it will be shown that at near light speeds, the modified Chameleon model produces a vortex structure aft of a moving object in the Chameleon (dark matter/energy) density field that has similarities to spacetime models as Warp-Drive and Wormholes.

Further, it will also be shown that the Chameleon vortex propulsion model is a natural extension of the interaction between Hawking and Unruh radiation, which provides a new roadmap toward new innovative space propulsion systems - that are founded in both nature and theory.

2. Vortex Current Structures In Nature

Birkeland [7, 8] proposed that magnetic disturbances accompanying the aurora boreal were caused by large electric currents flowing along the contours of the auroral zone, suggesting that the current entered from one end and left at the other, in a complete closed circuit. Although at the time the idea was not well accepted, in 1973 the Triad satellite have shown conclusively that the large-scale pattern of such (closed) currents do exist [9].

Different but related phenomena are the Herbig-Haro (HH) objects observed by Burnham [10]. HH objects are highly collimated, highly ionized matter ejections, which in the second author's viewpoint are propelled by a similar mechanism as presented above. For example, stars in their first hundred thousand years of existence are often surrounded by accretion disks build-up by gas (plasma, or just a good conductor) falling onto the black hole attracted by the strong gravitational field. The accretion disk is formed most probably because there is an oblate spheroid attracting particles. When particles fall into the center angular momentum flow outwardly, the proposed mechanism is MHD turbulence [11] as the accretion disks are not devoid of magnetic fields, and since they constitute a current of ionized particles falling into a black hole.

Kronenberg *et al.* [12] suggested that magnetic field lines (produced from closed astrological currents) extend a few million light years from galaxies into the intergalactic medium. Although the mechanism is not fully understood, the black hole accretion disk energy could be converted into magnetic fields through the agency of efficient energy-producing dynamos within black holes, a kind of cosmic electric motor. Occasionally black holes eject huge amounts of gas. In particular, blazars might expel jets of plasma into space, a phenomena observed by a team from the blazar BL Lacertae, the plasma jet spiraling outward from the flattened disk of spinning gas surrounding the supermassive black hole (Figure 1) extending 950 million light years beyond [13].

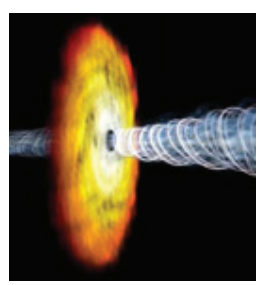

Figure 1. An artist concept of a spiraling (vortex) jet of high-energy particles (plasma) shooting out of the polar region of a supermassive black hole of a distant galaxy.

Newly forming ("pre-T-Tauri") stars are usually surrounded by bipolar jets and molecular outflows in regions with small patches of nebulosity associated with newly born stars (*i.e.*, Herbig-Haro objects). Several models have been proposed to explain jet ejection-accretion processes and it is becoming evident that pure hydrodynamical models are not sufficient, and most probably MHD magneto-centrifugal ejection seems at the source of the driving mechanism [14]. Optical observations [15] indicates that jets are produced in regions 5.5 AU in diameter, while attaining distances 800 AU in length and widths with Mach angles typical for free lateral expansion of a supersonic jet.

These references concur to the general view that closed currents pervade the entire universe and, in particular, there is a cosmic mechanism to expel matter to large astronomical distances involving vortex currents with similarities to the vortex shown in Figure 1. Therefore, one should suspect other similarities in nature at the terrestrial level involving force producing vortices. In fact, Dickinson [16], with further discussion by the second author [1], has shown that the main propulsion mechanism in nature relies on the production of vortices for some material structures (*e.g.*, wing, duck paddles, fish's tail) as shown in Figure 2. That is, fishes swim by flapping their tail and other fins, and squid and salps, eject fluid intermittently as a jet, producing optimal vortex rings which give the maximum thrust for a given energy input [17]. Also, quite interestingly, their trajectory is done by crossing the vortex produced at each stroke, like traveling through a channel of vortices.

Figure 2. Locomotion in fluids and vortical structure generated at each stroke by bird and fish [1].

3. The Chameleon Model

The Chameleon Theory [5, 6] represents a fifth force of nature. This fifth force is given as a Chameleon (*i.e.*, hiding within known physics) scalar field tied to the density of matter by way of a thin-shell concept or mechanism. Such an analogy gives the Chameleon field dark energy/dark matter like characteristics [4, 18, 19]; fitting well within the cosmological expansion [2] and provides a mechanism to carry currents throughout the Universe.

The foundation of the thin-shell mechanism was developed by concentrating on the static solution *where time fluctuations are set to zero* within and about a spherically symmetric and significantly large object of homogeneous density ρ_m, mass m and radius R_m having a thin shell thickness ΔR_m. The thin shell model is illustrated in Figure 3, where the thin-shell thickness $\Delta R_m << R_m$ (shown large in the figures for clarity) and where the arrows represent the Universe acceleration (*i.e.*, expansion) of the Chameleon field.

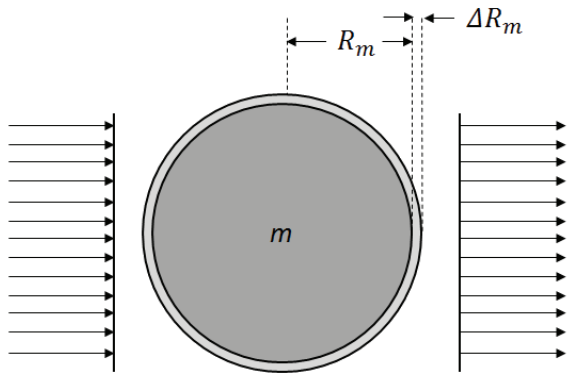

Figure 3. Chameleon thin-shell model.

The first author [2] showed that the thin shell thickness can be given by

$$\Delta R_m \approx \frac{1}{3}\left(\frac{M_E^2}{\hat{\beta}_C R_m \rho_m}\right)\left(\frac{2M_{PL}^4}{\rho_0}\right)^{1/3}\left(1-\left(\frac{\rho_0}{\rho_m}\right)^{1/3}\right) \tag{1}$$

where $M_E \approx 10^4\ m^{-1}$ is the universe energy scale factor, $M_{Pl} = 4.34\times10^{-9}\ kg$ is the reduced Planck mass, $\hat{\beta}_C$ is the motion coupling factor to the external Chameleon field, ρ_0 is the external surrounding mass density.

For this paper, only cases where the external density ρ_0 ($<<\rho_m$ as is in most cases) and the mass m are constant, where equation (1) can be reduced to

$$\Delta R_m \approx \frac{4\pi}{9}\left(\frac{M_E^2}{m}\right)\left(\frac{2M_{PL}^4}{\rho_0}\right)^{1/3}\times\left(\frac{R_m^2}{\hat{\beta}_C}\right);$$

noting the thin shell thickness is solely a function of square of the radius R_m^2 divided by the motion factor $\hat{\beta}_C$. Then with $\hat{\beta}_C \sim 1$ (earth case), equation (1) indicates an object's thin shell will change as the square of its radius – *i.e.*, the thin shell thickness $\Delta R_m \propto R_m^2$. That is,

1) As the radius of an object gets smaller (increasing density) the thin shell gets smaller, or
2) As the radius of an object gets larger (decreasing density) the thin shell gets larger.

For example, the thin shell thickness of a sun with radius R_{sun} will be larger than the thin shell of a black-hole with the same mass, provided its radius $<< R_{sun}$. Generally, this infers that as the density of an object increases, the thin shell thickness decreases – *e.g.*, the collapse of a star to a black-hole.

3.1 Fifth Force Coefficient

The Chameleon theory implies a correction to the gravitational force as $F = (1+\theta)F_N$, where $F_N = mg$ is the standard force of gravity and $\theta = 6\beta_m\left(\Delta R_m / R_m\right)$ is the fifth force coefficient, where β_m is the object's coupling factor to the external Chameleon field. The fifth force F_m on an object of mass m and constant radius R_m is then given in terms of the coupling factor and the thin shell thickness as

$$F_m \approx \theta F_N = 6\beta_m \left(\Delta R_m / R_m\right) F_N . \tag{2}$$

Noting that the case under study,

$$F_m \approx \left(\frac{4\pi}{9} \left(\frac{M_E^2}{m} \right) \left(\frac{2M_{PL}^4}{\rho_0} \right)^{1/3} F_N \right) \times \left(\frac{\beta_m}{\hat{\beta}_C} R_m \right);$$

4. The Modified (Acceleration) Chameleon Model

The Modified Chameleon Model [2-4] is founded on the fact that *time fluctuations can exist within and about an object*, such that, densities can vary even if only slightly to cause changes in an object's internal or external Chameleon scalar field; affecting the thin shell thickness about an object. Noting that such fluctuations changes cannot change an objects mass – *i.e.*, only changes to the radius can occur. Then if the radius changes are induced linearly in the direction of motion, the thin-shell about an object will change accordingly. This is illustrated by an increase in the thin shell thickness in the direction of motion and a decrease in the thin shell opposite to the direction of motion (illustrated in Figure 4).

Under this study, this implies that the fifth force on an object be given as

$$F_m \approx \left(\frac{4\pi}{9} \left(\frac{M_E^2}{m} \right) \left(\frac{2M_{PL}^4}{\rho_0} \right)^{1/3} F_N \right) \times \left(\frac{\beta_m}{\hat{\beta}_C} \delta R_m \right);$$

where δR_m is redefined as the Chameleon *radial factor* as it implies a change to the internal Chameleon field of an object and not the actual static density. It will be shown that changes in the radial factor also influences changes in the mass coupling β_m and the motion coupling $\hat{\beta}_C$ as they are inner related.

4.1 External Chameleon Field Motion

With respect to the original Chameleon Theory, the modified Chameleon model also represents small variations in the gravitational force on an object due to motion of the external Chameleon Field about an object, which in general terms is represented by the acceleration of gravity g_M of the largest nearby object of mass M.

For example, the object of mass m in Figure 3 and the external Chameleon Field are both accelerated toward a larger object of mass $M \gg m$ as shown in Figure 4, here the arrows represent the gravitational acceleration of the Chameleon field. Noting that the external Chameleon Field is only minimally coupled (*i.e.*, $\beta_M \approx 1$) to the larger object. Here the smaller object of mass m is assumed to be at a fixed distance from the larger object of mass M. However, the external Chameleon Field mass m_C is free to move, such that the motion coupling factor $\hat{\beta}_C \neq 1$. That is, the fifth force per unit mass $m_C = 1\ kg$ of the Chameleon field is

$$\frac{F_M}{m_C} \approx 6\beta_M \left(\frac{\Delta R_M}{R_M} \right) \frac{F_N}{m_C} .$$

For the earth $(\oplus)$ with $\beta_\oplus \approx 1$, $\hat{\beta}_{C_\oplus} \approx 1$ and $F_{N_\oplus} = m_C g_\oplus$, $F_\oplus / m_C \approx 10^{-7}\ N/kg$. Of note, the earth example infers that when the object and the surrounding ambient field are both subject to the same acceleration, the motion factor $\hat{\beta}_C = 1$.

Now since the smaller object is in the moving external Chameleon Field, the small object's motion factor $\hat{\beta}_{C_m} \neq 1$ and produces a change $\delta\Delta R_m$ per equation (1) in the thin shell thickness of the smaller object as shown in Figure 4; predominately toward the larger object. That is, the motion of the external Chameleon Field mass toward the larger object compresses the smaller object's thin-shell outward (*aft*) and expands the thin-shell toward (*FW*) the larger object to keep the total energy in the thin-shell constant as the smaller object's density is unchanged. This produces a change in the thin-shell thicknesses about the smaller object, *i.e.*,

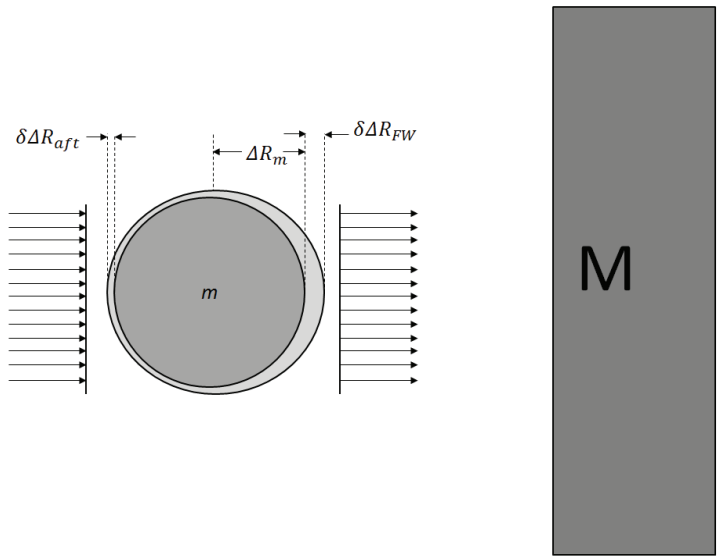

Figure 4. The Modified Chameleon Model.

$$\delta\Delta R_{aft} \approx \frac{4\pi}{9}\left(\frac{M_E^2}{m}\right)\left(\frac{2M_{PL}^4}{\rho_0}\right)^{1/3} \times \left(\frac{R_m^2}{\hat{\beta}_{aft}}\right);$$
$$\delta\Delta R_{FW} \approx \frac{4\pi}{9}\left(\frac{M_E^2}{m}\right)\left(\frac{2M_{PL}^4}{\rho_0}\right)^{1/3} \times \left(\frac{R_m^2}{\hat{\beta}_{FW}}\right).$$

Now since the changes $\delta\Delta R_m$ in the thin shell thickness of the smaller object produces an asymmetric thin-shell thickness about the smaller mass, disproportion more in the direction of the gravitational force of the larger object, the fifth force coefficients θ about the smaller object are no longer symmetric. Therefore, we must sum the fifth force coefficients $\sum\theta$, but only in the direction of motion (acceleration). Whereby the fifth force $\frac{1}{2}\sum\theta \cdot F_N \;\; F_N = mg_M$ on the smaller object effects its gravitational force according to $F_g = (1+\frac{1}{2}\sum\theta)F_N$, where the factor $\frac{1}{2}$ accounts for linearization of the force.

Then in this model, the fifth force F_m is given in terms of the changes in thin shell thickness $\delta\Delta R_m$ and changes in the mass to field coupling $\delta\beta_m$ (as it is inner related to the smaller object's motion factor) in the direction of (aft and forward) motion in like to equation (2) as

$$F_m \approx \tfrac{1}{2}\sum \theta F_N = 3\left(\frac{\delta\beta_{FW}\delta\Delta R_{FW} - \delta\beta_{aft}\delta\Delta R_{aft}}{R_m}\right)F_N . \tag{3}$$

4.1.1 The Chameleon Field Mass Coupling Factor and Inner Relationships

Now as before let $\rho_m \gg \rho_0$ (as is in most cases), where equation (1) gives the aft and forward changes in the thin shell thickness

$$\begin{aligned} \delta\Delta R_{FW} &\approx \frac{1}{3}\left(\frac{M_E^2}{\hat{\beta}_{C_{FW}} R_m \rho_m}\right)\left(\frac{2M_{PL}^4}{\rho_0}\right)^{1/3}; \\ \delta\Delta R_{aft} &\approx \left(\frac{\hat{\beta}_{C_{FW}}}{\hat{\beta}_{C_{aft}}}\right)\delta\Delta R_{FW} . \end{aligned} \tag{4}$$

During the development of this model, it was found that for the earth,

$$\Delta R_m \approx \beta_m^2 \sqrt{l_p R_m} , \tag{5}$$

where the Chameleon Field mass coupling $\beta_m \approx 1$ for the Earth in the original Chameleon Theory. Combining equation (5) with equations (4) yields the Modified Chameleon field mass coupling factors as

$$\begin{aligned} \beta_{FW} &\approx \left(\left(\frac{1}{3}\left(\frac{M_E^2}{\hat{\beta}_{C_{FW}} \rho_m \sqrt{l_p R_m^3}}\right)\left(\frac{2M_{PL}^4}{\rho_0}\right)^{1/3}\right)\right)^{1/2}; \\ \beta_{aft} &\approx \left(\frac{\hat{\beta}_{C_{FW}}}{\hat{\beta}_{C_{aft}}}\right)^{1/2} \beta_{FW} \approx \left(\frac{\delta\Delta R_{aft}}{\delta\Delta R_{FW}}\right)^{1/2} \beta_{FW} . \end{aligned} \tag{6}$$

To give the inner relationships as

$$\left(\frac{\beta_{aft}}{\beta_{FW}}\right)^2 \approx \frac{\delta\Delta R_{aft}}{\delta\Delta R_{FW}} \approx \frac{\hat{\beta}_{C_{FW}}}{\hat{\beta}_{C_{aft}}} .$$

*****

Example – For the earth ($\oplus$), the modified and unmodified Chameleon models must give similar results. That is, for $\hat{\beta}_C = 1$, $\beta_{\oplus_{aft}} = \beta_{\oplus_{FW}} \to 1$; whereby $\delta\Delta R_{FW} = \delta\Delta R_{aft} \to \Delta R_m \approx \sqrt{l_p R_m} \approx \left(1/3\left(M_E^2/R_m\rho_m\right)\left(2M_{PL}^4/\rho_0\right)^{1/3}\right)$, which implies that

$$l_p \approx \left(\frac{1}{\rho_m^2 R_m^3}\right) \times \left(\frac{1}{3} M_E^2 \left(\frac{2M_{PL}^4}{\rho_0}\right)^{1/3}\right)^2 ,$$

where $l_p \approx 1.616252\times10^{-35}\ m$. For the earth with $\rho_\oplus = 5520\ kg/m^3$, $R_\oplus \approx 6383.5\ km$ and $\rho_0 \approx \frac{1}{2}\rho_{atm@see-level} \approx 0.57\ kg/m^3$ gives $l_p = 1.6178\times10^{-35} m$.

4.1.2 Chameleon Field Lines in the Modified Chameleon Model

It is noted that by mapping the thin-shell thickness at specific distances r from the center of an object effectively produces field lines. In the original Chameleon Theory, equation (1) would only produce concentric rings about the object. In the Modified Chameleon model, equations (4) or (5), the distance between field lines shrink or expand with respect to the change $\delta\Delta R_m$ in the thin-shell thickness. Field lines will be illustrated later in the paper.

5. Internal Chameleon Field Changes: Density Excitation Model

As in the original Chameleon Theory, in the modified Chameleon model, the internal Chameleon field density of an object is defined as the object's density ρ_m. The difference is that in the modified Chameleon model, an object's internal Chameleon field density change $\delta\rho_m$ can produce similar motion effects on an object - *to that shown in Figure 4 on the smaller object due to the acceleration of gravity* - without the presence of an external large object. To do this, equation (4) is written as

$$\begin{aligned}\delta\Delta R_{FW} &\approx 1/3\left(M_E^2/\hat{\beta}_{C_{FW}}\delta R_m\delta\rho_m\right)\left(2M_{PL}^4/\rho_0\right)^{1/3}\\ \delta\Delta R_{aft} &\approx \left(\hat{\beta}_{C_{FW}}/\hat{\beta}_{C_{aft}}\right)\delta\Delta R_{FW}\end{aligned}, \tag{7}$$

where the change $\delta\rho_m$ in an object's internal Chameleon field density also produced a change in the Chameleon field radius δR_m. Then from equation (6), the inner relationships are re-established as

$$\left(\frac{\delta\beta_{aft}}{\delta\beta_{FW}}\right)^2 \approx \frac{\delta\Delta R_{aft}}{\delta\Delta R_{FW}} \approx \frac{\hat{\beta}_{C_{FW}}}{\hat{\beta}_{C_{aft}}};$$

noting that the motion coupling factors will change according, but are left as is as they are already assumed to change in the Modified Chameleon model.

This then produces the Chameleon Field mass coupling from equation (6) as

$$\begin{aligned}\delta\beta_{FW} &\approx \left(\frac{1}{3}\left(\frac{M_E^2}{\hat{\beta}_{C_{FW}}\delta\rho_m\sqrt{l_p\delta R_m^3}}\right)\left(\frac{2M_{PL}^4}{\rho_0}\right)^{1/3}\right)^{1/2};\\ \delta\beta_{aft} &\approx \left(\frac{1}{3}\left(\frac{M_E^2}{\hat{\beta}_{C_{aft}}\delta\rho_m\sqrt{l_p\delta R_m^3}}\right)\left(\frac{2M_{PL}^4}{\rho_0}\right)^{1/3}\right)^{1/2},\end{aligned} \tag{8}$$

differing only by the motion coupling factors.

5.1 Density Excitation and Radius Change

The object's field density change is given by

$$\delta\rho_m \approx \left(1+a_m\right)\rho_m + \left(a_i/g_m\right)\rho_i = 3m\Big/\left(4\pi\cdot\delta R_m^3\right) \tag{9}$$

where a_i is the acceleration of the internal particulate matter in the direction of motion, noting that the object's acceleration a_m and the internal particulate matter acceleration a_i are not necessarily equal.

The author notes that the internal particulate matter needs to be coherent, which typically requires that internal particulate matter be no bigger than subatomic particles as atoms and larger matter become subject to large scale random collisions, which reduces the overall coherence – effecting the total density change in the object. Exclusion to this is the standard rocket model [4], where large scale mass coherence occurs in the nozzle. Current examples of experimental devices that have produced excitation of internal particulates include work by: Brito [20]; Feigel [21]; Shawyer [22]; Woodward [23, 24], which generally excite electron/photon motion within materials.

Equation (10) yields the object's changed field radial factor

$$\delta R_m = \left(\left(1+a_m+a_i/g_m\left(m_i/m\right)\right)^{-1}\right)^{1/3} R_m; \tag{10}$$

remembering that the radial factor δR_m implies that the object's internal Chameleon field density footprint decreases, not its actual matter radius and that $\delta R_m \to R_m$ as $a_i \to 0$ and $a_m \to 0$.

5.2 Phase Factor and Mass Coupling Factor

The uniqueness of the Density Excitation Model is that it circumvents the need for determining the motion factors. This is achieved by the fact that an object's Chameleon field density change $\delta\rho_m$ is due to the acceleration of internal particulate matter of mass m_i, where the internal particulate matter never leaves the object, but relaxes back into the object over its normal relaxation time between impulses and implies a linear or directional phasing φ of the density.

Typically, the phasing is relativistic as internal particulate matter must be atomically small to move inside the matter matrix of the object without destroying the object. Whereby for example, the phase for electrically exited particulates can be given as

$$\varphi \approx 1 - v_{relax}/c, \tag{11}$$

where v_{relax} is the relaxation velocity of the accelerated particulate matter back into the object [4], where the forward mass coupling factor is given as

$$\delta\beta_{FW} \approx \left(\frac{m_s a_m + m_i a_i}{\left(m_s - m_i\right)g_m}\right)\frac{1}{6\varphi}; \tag{12}$$

noting that the aft mass coupling factor $\delta\beta_{aft}$ is given by from equation (7) in terms of the thin-shell thicknesses $\left(\delta\Delta R_{aft}\ \&\ \delta\Delta R_{FW}\right)$ and the forward mass coupling factor $\delta\beta_{FW}$.

6. The Far-Space Propulsion Example

Consider a spaceship far from any large masses with mass $m_s = 10^4\ kg$, effective radius $R_s = 10\ m$, density $\rho_s \approx 2.387\ kg/m^3$, and where $\rho_0 = \rho_c \sim 1.11778x10^{-26}\ kg/m^3 \ll \rho_s$. In far space with no internal Chameleon density change, the spaceship is accelerating with the background (Universe) expansion, such

that, the spaceship's motion coupling factor $\hat{\beta}_C = 1$. Therefore the spaceship Chameleon field coupling factor β_s is then given from equations (6) as $\beta_s \approx 2.09x10^{10}$. Then from equation (4) with $\rho_0 << \rho_m$, the spaceships thin shell thickness $\Delta R \approx 5.567x10^3\ m$.

Also in far space, the nearest gravity source is the spaceship itself where $F_N = m_s g_s$. Here $g_s = G \cdot m_s / R_s^2 = (4\pi/3) R_s G \rho_s \approx 6.674x10^{-9}\ m/s^2$, such that, $F_N \approx 6.674x10^{-5} N$.

6.1 Far-Space Coupling

Now consider that the spaceship has the capability to modulate its density through the excitation of internal particulates of total mass $m_i = 10^{-4} m_s = 1\ kg$. Since the particulate matter has the same effective radius as the spaceship, the particulate matter's density $\rho_i \approx 10^{-4} \rho_s$. Then given the spaceship at rest $a_s = 0$ with a particulate matter forward acceleration $a_i = c/2s \approx 1.5x10^8\ m/s$; using equations (9) and (10), the spaceship density change $\delta\rho_s \approx 5.362x10^{12}\ kg/m^3$ and radial footprint change $\delta R_s \approx 7.636x10^{-4}$ m.

Now letting the particulate matter relaxation velocity $v_{relax} = \frac{1}{2}c$ gives the phase $\varphi = \frac{1}{2}$ from equation (11). Then for the spaceship at rest where the acceleration $a_s = 0$, the spaceship forward field coupling factor change

$$\delta\beta_{FW} \approx \left(\frac{m_i}{(m_s - m_i)}\right)\left(\frac{a_i}{g_m}\right)\frac{1}{6\varphi} = 7.487 \times 10^{11}$$

from equation (12). That is, the coupling to the Chameleon field forward the spaceship is ~36 times stronger than when the particulate matter is not accelerating. Using equation (4) the forward thin shell change is $\delta\Delta R_{FW} \approx 6.227x10^4\ m$, which is more than a factor of 10 over the non-motion thin shell thickness of $\Delta R \approx 5.567x10^3\ m$ about the spaceship. Then from equation (3) with $\delta\beta_{FW}\delta\Delta R_{FW} \gg \delta\beta_{aft}\delta\Delta R_{aft}$, as it should be for this case, the fifth force is given as

$$F_s \approx 3\delta\beta_{FW}\left(\delta\Delta R_{FW}/\delta R_s\right)F_N .$$

Given the values established above, the fifth force $F_s \approx 1.223 \times 10^{16} N$.

6.2 Impulse Thrust

The Chameleon field force F_m does not actual define the actual thrust on the spaceship, which needs to be proportioned against the total impulse time t per pulse time dt and the particulates under acceleration, where such proportionality will need to be determined from experimental data.

However, as this is an acceleration-density model the impulse thrust T_{IP} is expected to be proportioned with respect to the accelerations and densities and range as

$$T_{IP} \approx \left(\frac{t}{dt}\right)\left(\frac{g_m}{a_m + a_i}\right)F_m \rightarrow \left(\frac{t}{dt}\right)\left(\frac{g_m}{a_m + a_i}\right)\left(\frac{\rho_m}{\rho_i}\right)F_m ,$$

where for the spaceship example in far space with $t/dt = 1$, the impulse thrust $T_{IP} \approx 0.544N \rightarrow 5{,}440N$ for $a_s = 0$. Noting that the thrust decreases as the spaceship accelerates for a constant particulate mass acceleration a_i.

7. Chameleon Field Mapping about an Accelerating Spaceship

If the spaceship accelerates, say $a_s \to a_i = \frac{1}{2}c$, then the spaceship factors: $\delta\beta_{FW} \approx 7.488x10^{15}$; where $\delta\Delta R_{FW} \approx 6.229x10^{12}\ m$. Increasing the forward thin-shell thickness by a factor of 10^8. Then per equation (6)

$$\delta\Delta R_{aft} \approx \left(\delta\beta_{aft}^2 \Big/ \left(7.488x10^{15}\right)^2\right) 6.229x10^{12}\ m = 1.111\times10^{-19}\,\delta\beta_{aft}^2,$$

where since

$$\delta\beta_{FW}\delta\Delta R_{FW} \approx 4.664\times10^{28} \gg \delta\beta_{aft}\delta\Delta R_{aft} \approx 1.111\times10^{-19}\,\delta\beta_{aft}^3$$

$$\delta\beta_{aft}^3 \ll \frac{4.664\times10^{28}}{1.111\times10^{-19}} = 4.198\times10^{47} \Rightarrow \delta\beta_{aft} \ll 7.488\times10^{15} \approx \delta\beta_{FW}$$

to insure $\delta\beta_{FW}\delta\Delta R_{FW} \gg \delta\beta_{afi}\delta\Delta R_{aft}$.

7.1 Gravitation Compression and Expansion

It can easily be seen from equation (1) that for a constant mass, as the radius R_m decreases the thin-shell thickness ΔR_m also deceases, but by the square R_m^2 of the radius. Given that the acceleration of gravity $g_m = Gm/R_m^2$ increases as the square R_m^2 of the radius decreases, a decreasing thin-shell thickness indicates gravitational compression while an increasing thin-shell thickness indicates a gravitational expansion. Applying this to the Modified Chameleon Model with a modulated internal Chameleon field (*i.e.*, particulate mass) produces the spaceship (of mass m) concept shown in Figure 5. As shown, gravitational expansion extends the forward thin shell in a conic fashion as it is connected to the spaceship while gravitational compression of the aft thin shell flattens the thin shell against the spaceship.

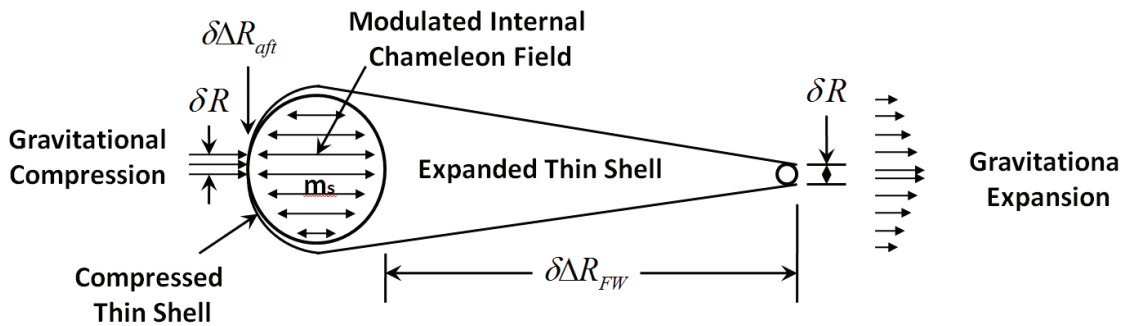

Figure 5. Gravitational Coupling of the External Chameleon Field Forward and Aft of a Spaceship of Mass m_s

7.1.1. Vortex Formation In The Wake Of The Chameleon Field

Now placing the affects given in Figure 5 into the Universe Chameleon field as illustrated in Figure 6, the accelerated field lines are shown to extend in the forward direction and contract in the aft direction. Since the field lines do not inner the object, but go around, there exist a toroidal void or annular vortex field aft of the spaceship above and below the radial area defined by δR. This is similar to the wake

behind an object traveling through any gases or fluid medium. Similarly, another annular vortex field void is produced forward the object near the forward thin-shell change $\delta\Delta R_{FW}$. It is noted that the forward annular vortex field is unstable as the field lines do not completely enclose the annular vortex field.

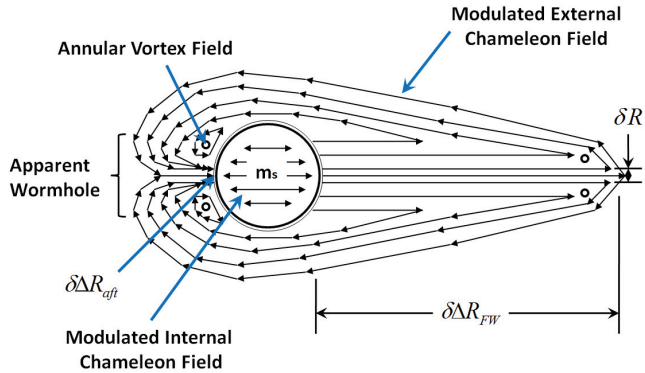

Figure 6. Spaceship of Mass m Traveling through the Universe Chameleon Field at Light Speed.

That is, from the standpoint of known physics, the motion of the spaceship must be somehow grounded to natural phenomena. In the wake aft of the spaceship mass (m_s) in Figure 6, the Chameleon field lines forms a toroidal or vortical structure about the Chameleon field lines interring the reduced radial area defined by δR. Since the field lines about the aft toroid are closed, they represent the thin shell about virtual mass. By assuming that this virtual mass are electron like, one can then assume that there is an inward force on the annulus due a Chameleon Magnus effect that squeezes the Chameleon field lines interring the reduced radial area. This is the Chameleon field analogy to pinching in magnet-current phenomena (as in electromagnetically pinched plasma) and provides an action force on the aft thin shell of the spaceship in the direction of motion, which in turn implies a force on the forward thin shell in the direction of motion – *i.e.*, cause an effect.

Further, due to the curvature of the Chameleon field about the annular vortex field, the rotating toroid has an upward and aft-ward force exerted on it, which forces the toroid away from the spaceship mass, only to reform a new toroid as the older one moves away. This is the Chameleon field analogy to the locomotion in fluids by vertical structures generated at each stroke by a bird or fish as shown in Figure 2.

8. Similarities To Conventional Propulsion

Similarities of the modified Chameleon model can be found in conventional propulsion. For example, similarities to conventional rocketry are shown in Figure 7 with respect to Figure 5. As shown, the accelerated exhaust between the nozzle and the shock diamond represent the modulated Chameleon field with the nozzle throat and shock diamond representing the gravitational expansion and compression. Whereby, the thin-shell expansion in the nozzle is the force mechanism. An annular Vortex field is not present as the velocity of the modulated Chameleon field is much-much less than light speed.

These similarities exist even though the mass flow from the rocket is opposite the particulate matter flow in the mass of Figure 5. This reversal is due to the matter in the mass flow being greater than subatomic particles, whereby the sign on the Chameleon field pressure is reversed while the other physical characteristics remain the same.

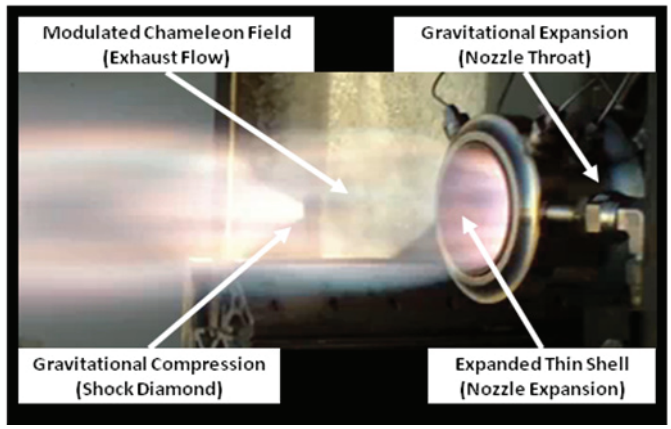

Figure 7. Similarities to Conventional Rocketry.

It is noted that the repetition of shock diamonds as seen in rocket exhausts would also be seen by an observer watching the flyby of a spaceship using the particulate mass changing density method of the modified Chameleon model. However, the radiation may not be visible to humans, but at some other wavelength as that of Hawking-Unruh radiation discussed later.

An example of the similarities related to the wake behind an object moving through an external Chameleon (density) field (*i.e.*, atmosphere) is shown in Figure 8, where aircrafts are shown breaking the sound barrier. As shown in Figures 8a, 8b and 8d, the shock patterns are distinctively behind the moving aircrafts, in similar to the vortex field in Figure 6. Noting that, the patterns are respectively larger than that illustrated in Figure 6 due to the denser external field. Also of note, Figure 8c shows the shock pattern a sonic aircraft, where the outward indention in the shock pattern represents the field expansion and the aft side indention toward the exhaust represents the field compression, similar to that in Figure 5. Further, by drawing lines perpendicular to the shock lines, one could trace out the Chameleon field lines similar to those about the spaceship in Figure 6. Finally, Figure 8d shows the existence of vortex formation in the aft field.

9. Warp-Drive And Wormhole Analogies

The annular vortex field in Figure 6 formed aft of the spacecraft and its similarity to natural vortex structure as shown in Figure 2 present characteristics to both Warp Bubbles (Figure 8) and Wormholes (Figure 10); for general references see [25]. These characteristic similarities are discussed in the following. Noting that, the authors do not claim faster than light in the Modified Chameleon Model, only that there is a resemblance.

10. Warp-Drive

From the standpoint of spacetime, where in Figure 5 the gravitational expansion forward the spaceship represents a gravity well (Contraction) and the gravitational compression of the thin shell aft of the spaceship represents a gravity hill (Expansion), the gravitational coupling of the external Chameleon fields have a resemblance to the Warp Bubble as shown in Figure 9. Noting that, for all practical purposes, the Alcubierre Warp Bubble laid down the preliminary ground work toward an active space drive within Einstein Physics, *i.e.*, spacetime [http://en.wikipedia.org/wiki/Alcubierre_drive].

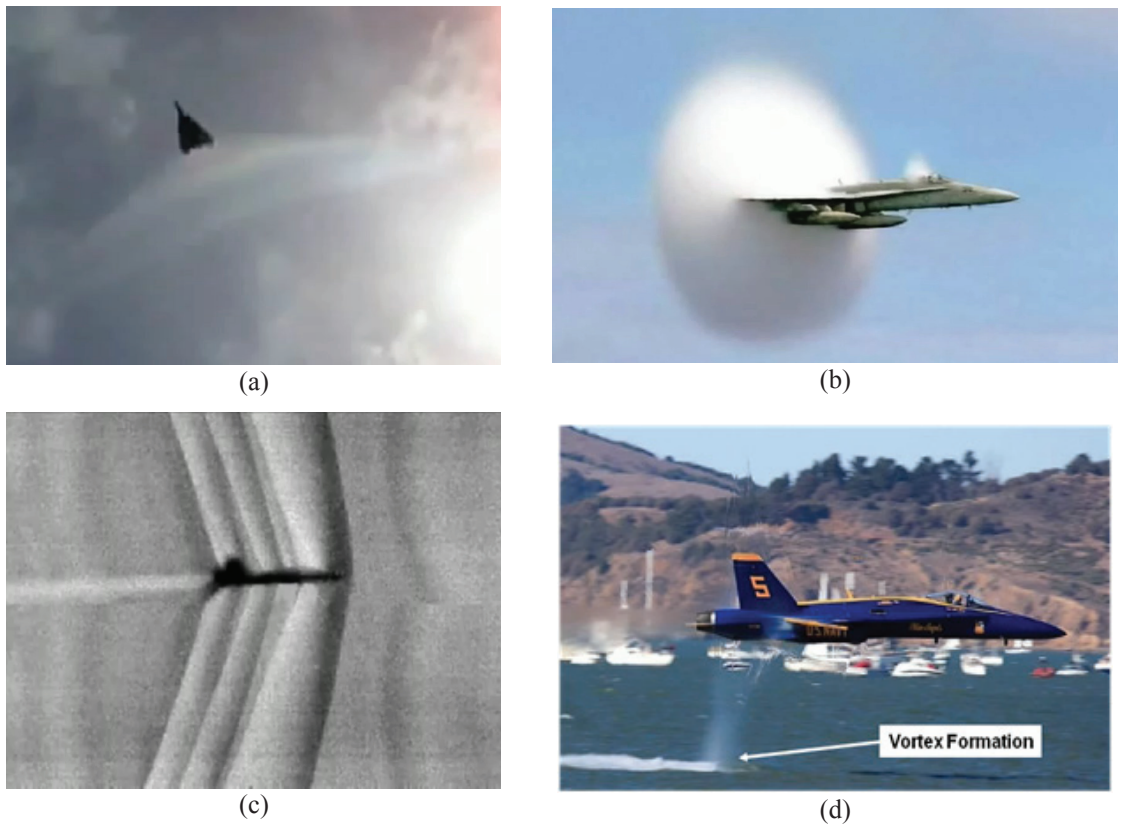

Figure 8. Similarities to Conventional Atmospheric Shock Formations.

This resemblance should not be surprising as the Chameleon Model [5, 6] is also based on Einstein Physics, but carries over to Quantum Field Theory within dark matter/energy models. Where dark matter/energy provides the source of exotic mass/energy required in WarpDrive Models.

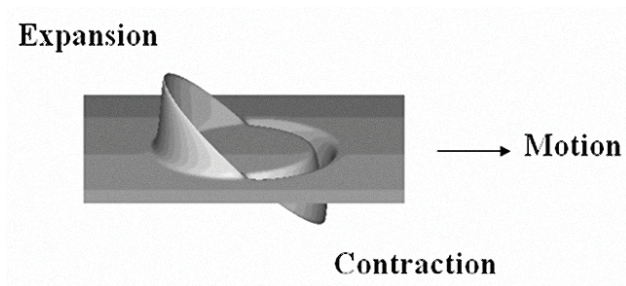

Figure 8. Alcubierre Warp Bubble.

11. Wormhole

In physics and fiction, a wormhole is a hypothetical topological feature of space time that would be, fundamentally, a "shortcut" through space time. Although wormholes are very popular in science fiction, there is no observational evidence. Although wormholes are valid solutions in general relativity, this is

only true if exotic matter can be used to stabilize them. Even if the wormhole is stabilized, it is believed that the slightest fluctuation in space would collapse it. Plus Wormholes allowed by current physical theories might arise spontaneously, but would vanish nearly instantaneously, and would likely be undetectable.

Figure 10 is an artist's impression of a wormhole from an observer's perspective, crossing the event horizon of a Schwarzschild wormhole, which is similar to a Schwarzschild black hole, but with the singularity replaced, by an unstable path to a white hole, in another universe [http://en.wikipedia.org/wiki/Wormhole]. The observer originates from the right, and another universe becomes visible in the center of the wormhole's shadow once the horizon is crossed; however, this new region is unreachable in the case of a Schwarzschild wormhole, as the bridge, between the black hole and the white hole, always collapses before the observer has time to cross it.

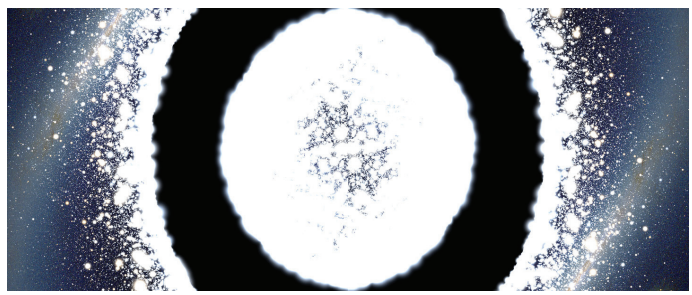

Figure 10. Event Horizon of a Schwarzschild Wormhole.

The authors note that the wormhole of Figure 9 has similarities to the aft view of Figure 6. These similarities are shown in Figure 11. As portrayed, the outer wormhole ring represents the annular Vortex field, the white distortion of space represents the externally modulated Chameleon field, and the distorted center of the wormhole represents the area of the radial change δR_{aft} .

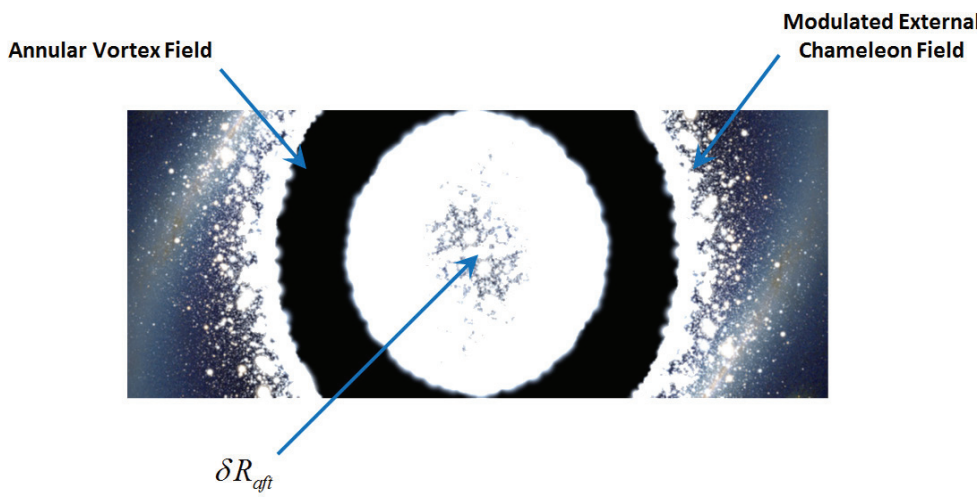

Figure 11. Aft View of a Spaceship Traveling through the Universe Chameleon Field at Light Speed.

12. Hawking-Unruh Radiation

The aft view of Figure 11 implies the emission of black hole or Hawking-Unruh radiation [26, 27], a measure of the quantum fluctuations in the radiation of accelerated charges from the aft of the spaceship.

Noting that, the difference between Hawking and Unruh radiation helps to clarify aspects of the equivalence between radiation in uniform acceleration and in a uniform gravitational field.

According to Hawking [26], an observer outside a black hole experiences a bath of thermal radiation of temperature

$$T_H = \frac{g}{2\pi k}\left(\frac{\hbar}{c}\right) \tag{13}$$

where g is the local acceleration due to gravity, c is the speed of light, $\hbar$ is Planck's constant and k $[1.3806503x10^{-23}\ m^2kg/s^2\ {}^0K]$ is Boltzmann's constant. Such that, Hawking radiation in some manner suggests that the background gravitational field interacts with the quantum fluctuations of the electromagnetic field with the result that energy can be transferred to the observer as if the observer were in an oven filled with black-body radiation. Of course, the effect is strong only if the background field is strong. An extreme example is that if the temperature is equivalent to 1 MeV or more, virtual electron-positron pairs emerge from the vacuum into real particles.

With respect to Hawking radiation, Unruh [27] suggested that this phenomenon can be demonstrated in the laboratory according to the principle of equivalence: an accelerated observer in a gravity-free environment experiences the same physics (locally) as an observer at rest in a gravitational field. Therefore, an accelerated observer (in zero gravity) should find them self in a thermal bath of radiation characterized by temperature

$$T_U = \frac{a}{2\pi k}\left(\frac{\hbar}{c}\right) \tag{14}$$

where a is the acceleration as measured in the observer's instantaneous rest frame.

12.1 Hawking-Unruh Propulsion

With respect to this paper, the difference in the Hawking and Unruh radiation infers that for a spaceship far from other objects with acceleration a_s and self gravity attraction g_s, that

$$\frac{a_s}{g_s} = \frac{T_U}{T_H} \tag{15}$$

Whereby, the thrust on the spaceship arises from the difference in the forward Unruh radiation and the aft Hawking radiation, which is given by

$$Thrust = m_s a_s = m_s\left(\frac{T_U}{T_H}\right)g_s \tag{16}$$

That is, by changing the natural thermal Hawking radiation T_H to Unruh radiation T_U about an object, you can make it move. This is illustrated in Figures 5 and 6, where the gravitational compression of the thin shell produces a temperature change in the region of the radial change δR_{aft} corresponding to the Unruh radiation of equation (19). Such that, virtual electron-positron pairs, absorbed by the gravitational expansion forward of the spaceship emerge from the annular vortex field as real particles. From this prospective, these real particles are exhausted as normal mass and provide the same thrust mechanism as in normal rocket propulsion.

13. Conclusion

A vortex formation in nature leads to natural propulsive methods. These are seen both at the cosmological scale in such things as blazars and black holes that eject matter to great astrological distances and at the terrestrial level in birds and fishes to propel the environmental fluids (mass) about them. In the Chameleon vortex theory presented in this paper, it is shown that vortex structure behind an accelerating spaceship acquires wormhole like similarities with an overall Warp-Drive appearance. These characteristics provide a method where differences in Hawking and Unruh radiation provides the propulsive method for space travel where virtual electron-positron pairs, absorbed by the gravitational expansion forward of the spaceship emerge from the annular vortex field aft of the spaceship as real particles, in-like to propellant mass ejection in conventional rocket theory.

Acknowledgement

The authors would like to thank the support of Dr. R. Lewis, Penn State Retired.

References

1. M. J. Pinheiro, Electromagnetotoroid Structures in Propulsion and Astrophysics. in the proceedings of *Space, Propulsion & Energy Sciences International Forum* (SPESIF-10), edited by G. A. Robertson, AIP CP1208, Melville, New York, 2010.
2. G. A. Robertson, Engineering Dynamics of a Scalar Universe, Part I: Theory & Static Density Models. Lecture Series paper in the proceeding of *Space, Propulsion & Energy Sciences International Forum* (SPESIF-09), edited by G. A. Robertson, AIP CP1103, Melville, New York, 2009.
3. G. A. Robertson, Engineering Dynamics of a Scalar Universe, Part II: Time-Varying Density Model & Propulsion. Lecture Series paper in the proceedings of *Space, Propulsion & Energy Sciences International Forum* (SPESIF-09), edited by G. A. Robertson, AIP CP1103, Melville, New York, 2009.
4. G. A. Robertson, The Chameleon Solid Rocket Propulsion Model. in the proceedings of *Space, Propulsion & Energy Sciences International Forum* (SPESIF-10), edited by G. A. Robertson, AIP CP1208, Melville, New York, 2010.
5. J. Khoury and A. Weltman, Chameleon cosmology. *Phys. Rev. D* 2004 **69**:044026.
6. J. Khoury and A. Weltman, Chameleon Fields: Awaiting Surprises for Tests of Gravity in Space. *Phys. Rev. Lett.* 2004 **93**:171104.
7. K. Birkeland, *The Norwegian Aurora Polaris Expedition 1902-1903*. H. Aschehoug & Co, Leipzig, 1908.
8. P. Carlqvist, Cosmic electric currents and the generalized Bennett relation. *Astrophys. Space Sci.* 1988 **144**:73-84.
9. T. A. Potemra, Observation of Birkeland Currents with the TRIAD Satellite. *Astrophysics and Space Science* 1978 **58(1)**:207-226.
10. S. W. Burnham, Note on Hind's Variable Nebula in Taurus. *Monthly Notices of the Royal Astronomical Society* 1890 **51**:94–95.
11. E. Priest and T. Forbes, *Magnetic Reconnection*. Cambridge University Press, Cambridge, 2000, p. 442.
12. P. P. Kronenberg, Q. W. Dufton, H. Li and S. A. Colgate, Magnetic energy of the intergalactic medium from galactic black holes. *Astrophys. J.* 2001 **560**:178-186.
13. A. P. Marscher, *et al.*, The inner jet of an active galactic nucleus as revealed by a radio-to-γ-ray outburst. *Nature* 452 2008 966-969.
14. S. Cabrit, Jets from Young stars. *Lect. Notes Phys.* 2007 **723**:21-53.
15. P. Hartigan, S. Edwards, and R. Pierson, Infrared Emission Lines of Fe II. as Diagnostics of Shocked Gas in Stellar Jets. *Ap. J.* 2004 **614**:L69.
16. M. Dickinson, Animal Locomotion: How to walk on water. Nature 2003 **424**:621-622.
17. P. F. Linden and J. S. Turner, Optimal vortex rings and aquatic propulsion mechanisms. *Proc. R. Soc. Lond. B* 2004 **271**:647–653.
18. P. Brax, C. van de Bruck, A.-C. Davis, J. Khoury, and A. Weltman, Detecting dark energy in orbit: The cosmological chameleon. *Phys. Rev. D* 2004a **70**:123518.
19. P. Brax, C. van de Bruck, A.-C. Davis, J. Khoury and A. Weltman, Chameleon Dark Energy. in *Phi in the Sky: The Quest for Cosmological Scalar Fields*. AIP CP736 2004b 105-110.
20. H. H. Brito, Experimental status of thrusting by electromagnetic inertia manipulation, *Acta Astronautica* 2004 **54**:547-558.
21. A. Feigel, Quantum Vacuum Contribution to the Momentum of Dielectric Media. *Phys. Rev. Lett.* 2004 **92(2)**:020404-1.
22. R. Shawyer, Microwave Propulsion – Progress in the EMDrive Programme. In the proceedings of the *International Astronautical Congress* IAC08-C4.4.7 2008.
23. J. F. Woodward, Investigation of Propulsive Aspects of Mach Effects. In the proceedings of the *Space, Propulsion and Energy Sciences International Forum* (SPESIF-09), edited by G. A. Robertson, AIP CP1103, Melville, New York, 2009.

24. J. F. Woodward, A Test for the Existence of Mach Effects With a Rotary Device. In the proceedings of *Space, Propulsion & Energy Sciences International Forum* (SPESIF-10), edited by G. A. Robertson, AIP CP1208, Melville, New York, 2010.
25. G. A. Robertson, P. A. Murad and E. Davis, New Frontiers in Space Propulsion Sciences. *Energy and Conversion Management* 2008 **49**:436-452.
26. S. W. Hawking, Black Hole Explosions. *Nature* 1974 **248**:30-31
27. W. G. Unruh, Notes on Black Hole Evaporation. *Phys. Rev. D* 1976 **14**:870-892.